The Astrophysical Journal, 774:71 (7pp), 2013 September 1 doi:10.1088/0004-637X/774/1/71

ON THE COMBINATION OF IMAGING-POLARIMETRY WITH SPECTROPOLARIMETRY OF UPPER SOLAR ATMOSPHERES DURING SOLAR ECLIPSES

Z. Q. Qu[1], L. H. Deng[1,2], G. T. Dun[1,2], L. Chang[1,2], X. Y. Zhang[1], X. M. Cheng[1,2], J. Allington-Smith[3], G. Murray[3], Z. N. Qu[1,2], Z. K. Xue[1,2], and L. Ma[1,2]
[1] Yunnan Astronomical Observatory, Chinese Academy of Sciences, Kunming, Yunnan 650011, China
[2] Key Laboratory for the Structure and Evolution of Celestial Objects, Chinese Academy of Sciences, Kunming, Yunnan 650011, China
[3] Center for Advanced Instrumentation, University of Durham, UK
Received 2013 March 26; accepted 2013 July 1; published 2013 August 19

ABSTRACT

We present results from imaging polarimetry (IP) of upper solar atmospheres during a total solar eclipse on 2012 November 13 and spectropolarimetry of an annular solar eclipse on 2010 January 15. This combination of techniques provides both the synoptic spatial distribution of polarization above the solar limb and spectral information on the physical mechanism producing the polarization. Using these techniques together we demonstrate that even in the transition region, the linear polarization increases with height and can exceed 20%. IP shows a relatively smooth background distribution in terms of the amplitude and direction modified by solar structures above the limb. A map of a new quantity that reflects direction departure from the background polarization supplies an effective technique to improve the contrast of this fine structure. Spectral polarimetry shows that the relative contribution to the integrated polarization over the observed passband from the spectral lines decreases with height while the contribution from the continuum increases as a general trend. We conclude that both imaging and spectral polarimetry obtained simultaneously over matched spatial and spectral domains will be fruitful for future eclipse observations.

Key words: polarization – Sun: chromosphere – Sun: corona

1. INTRODUCTION

It is well known that magnetic field plays a crucial role in controlling the behavior of plasma in the upper solar atmosphere (corona, transition zone, and upper chromosphere), but we still do not fully understand the magnetic configuration and therefore the physical mechanisms in these layers. Furthermore, though we know the physical conditions in the upper solar atmosphere deviate further and further from thermodynamical equilibrium as height increases, we do not fully comprehend the detailed microvelocity distribution of the particles there. All of these hinder us from really understanding the atmosphere.

Polarimetry is the most reliable tool for determining the magnetic field and other physical parameters, and solar eclipses supply a rare but very valuable opportunity to obtain precise measurements by minimizing the light contamination directly from the photosphere. The eclipse data have been used to derive, say, the electron density and characteristic temperatures (e.g., van de Hulst 1950; Kulijanishvili & Kapanadze 2005; Skomorovsky et al. 2012).

Generally, polarimetry during solar eclipses can be divided into two categories. Imaging polarimetry (IP) is used for wide-field imagery in specified filter passbands while spectropolarimetry (SP) produces spectra in polarized light using dispersing elements such as diffraction gratings. Examples of IP results include Schuster (1878), Ney et al. (1961), Blackwell & Petford (1966), Eddy & Malville (1967), Hyder et al. (1968), McDougal (1971), Koutchmy & Schatten (1971), Badalyan & Sýkora (1997), and more recently, e.g., Kulijanishvili & Kapanadze (2005), Kim et al. (2011), and Skomorovsky et al. (2012). The most striking fact revealed consistently by different authors via IP is that the upper solar atmosphere is strongly polarized. Qu et al. (2009), using SP, showed that strong polarization (35%) is also present in some flash spectra generated from the upper chromosphere and transition zone, and that the amplitude can vary greatly from one spectral line to another. In this paper, we combine both techniques to show that these two types of polarimetry are complementary and productive.

2. OBSERVATIONS

On 2012 November 13, a total solar eclipse belt swept across the northeastern part of Australia. The eclipse was observed using IP at Ellis Beach, north of Cairns, Queensland. The totality started at 20:38:19 UT, peaked at 20:39:21, and ended at 20:40:23 UT. An 80 mm aperture refractive telescope with a focal ratio of $f/8$ was used for the IP. A 20 mm diameter filter restricted the passband to be 10.0 nm wide, centered at 530.0 nm. This was followed by a 20 mm aperture polaroid, HN45, whose extinction ratio reaches 100:1.7 at 530 nm. The detector was a scientific-grade CMOS chip consisting of 2048×2048 pixels, each covering 2.4×2.4 arcsec.

Figure 1 shows the raw images when the transmission polarization direction of the polaroid was rotated 0°, 45°, and 90° with respect to the reference positive Stokes Q direction, which is 66°.5 anticlockwise from the west–east direction. Three panels (the upper left, upper right, and lower left panels) are for polarization states $1/2(I + Q)$, $1/2(I + U)$ and $1/2(I - Q)$. The exposure time for all these images was 5.0 ms, acquired at 20:39:33 UT, 20:39:53 UT, and 20:40:05 UT, respectively. We obtain Stokes I, Q, and U maps from these three images. Calibration of dark current and spatial uniformity (flat field) were also taken and the images spatially co-registered so that images with opposite polarization states could be added and subtracted to get Stokes I, Q, and U parameters, respectively. Data were discarded with measured intensity below a threshold of e (= 2.713) times the noise level 4.2. The polarimetric noise level was measured from the lunar disk, where the intrinsic polarization should be zero but found to be 4.37%. The derived Stokes I map is shown in the lower right panel in Figure 1 in which the dark disk extends to 1.05 solar radii above the limb. Figure 2 shows maps of the polarimetric results.

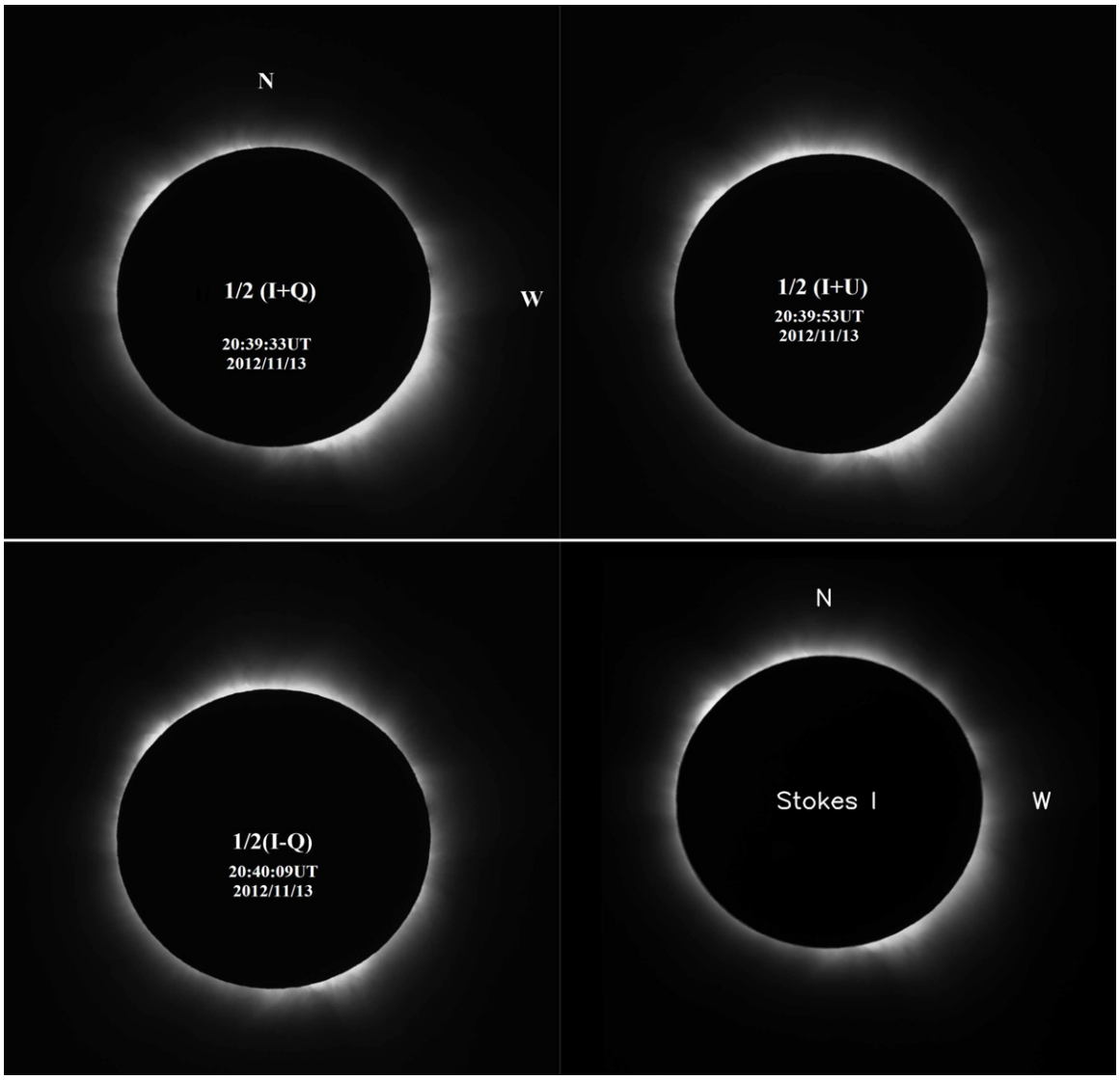

Figure 1. Raw imaging polarimetric data and derived Stokes *I* image (lower-right panel). The loops above the western limb and the outstanding prominence above the northern limb are used for spatial correlation to do further analysis.

On 2010 January 15, an annular solar eclipse took place, and SP was carried out just before the second contact at 8:40:35 UT at Erhai lake of Dali city, Yunnan province, China. The telescope, an equatorially mounted reflective telescope (Meade LX200GPS), and a fiber-fed spectrograph (PI SP2750) were the same as used during the total solar eclipse on 2008 August 1 (as detailed by Qu et al. 2009). The fiber array was aligned in two columns, each designed to be parallel to the slit, forming five polarimetric pairs (each fiber in the pair, having a numerical aperture of 0.20 mm, was illuminated respectively by orthogonally polarized ordinary and extraordinary beams from the same spatial origin in the solar atmosphere). Each fiber column was illuminated by one of the dual beams produced by a 1 cm thick calcite behind the slit, whose 0.12 mm wide extraordinary and ordinary images are projected onto the fiber array. The actual distance between the fibers in each pair varied from one pair to another due to an imperfect manufacturing process. Thus we have for these pairs different co-spatial factors, defined as the ratios of the common area illuminated, respectively, by the ordinary and extraordinary beams from the same spatial origin to their average illuminated area. It was found that the pair consisting of the fourth and eighth fibers, counted from the top to the bottom in each panel of Figure 3, was the best co-spatially matched among the five pairs, with a co-spatial factor of 94.6%. Thus only results from this pair were used in the subsequent analysis.

During the annular eclipse observation, the slit position was controlled manually and adjusted to be just above the cusp of the eclipse-formed sickle so that the highest contrast was available by minimizing stray light from the photosphere. The polarization direction of the ordinary beam is set to be parallel to the slit, and this defines the positive Stokes Q. Each fiber covered about 5.8 × 9.6 arcsec and the spectral coverage was 516.0–532.5 nm. A data set of 100 frames containing polarized spectral images was obtained with an exposure time of 1.0 s. Unlike the IP measurements, we obtained Stokes Q from dual beam analysis at each exposure. Five panels in Figure 3 illustrate these polarized flash spectra produced by the 10 fibers in five pairs at different times. The polarimetric precision is estimated in the lowest curve of lower right panel of Figure 4 whose amplitudes indicate the polarimetric error magnitude for each wavelength involved in the polarimetry. They are represented by

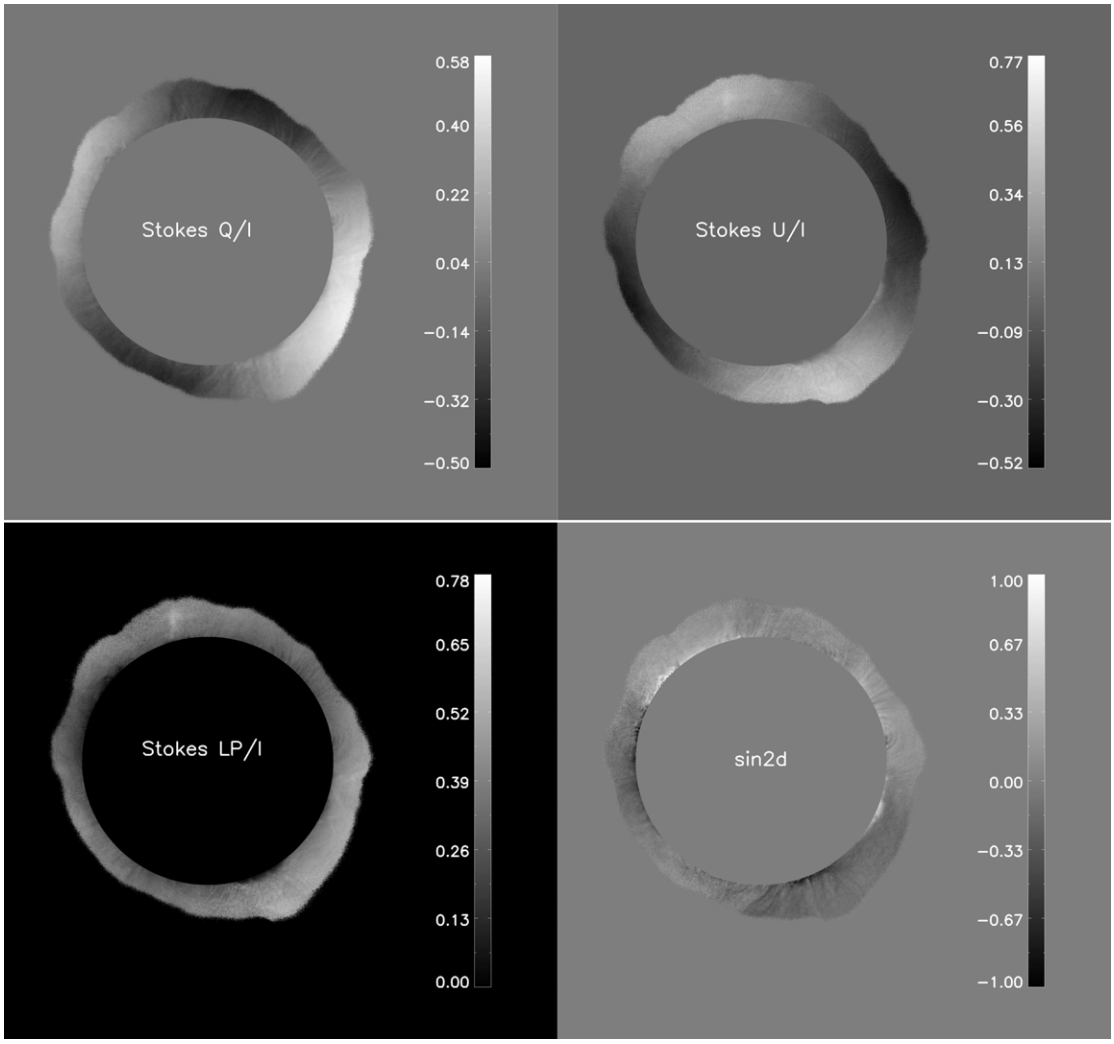

Figure 2. Maps of the derived polarization amplitudes represented by respectively Stokes Q/I, U/I and total linear polarization degree (Stokes LP/I), and map reflecting departure of polarization direction from the local tangent direction (bottom right panel). The polarimetry can reach 0.65 solar radius above the limb with a signal to noise ratio e.

the rms obtained from 18 frames when polarimetry was applied to the quiet Sun regions in the same data set. From this curve we estimate the polarimetric precision over the band to be 2.15% rms. Taking account of the co-spatial factors implies a 2.27% polarimetric precision, provided the polarization is uniformly distributed over each fiber.

We depict Stokes I/I_c and Q/I spectra in Figure 4 derived from the pair. The famous coronal green line, Fe XIV 530.3 nm, was not detected, which suggests that the SP missed the corona. But the singly ionized neodymium line Nd II 531.98 nm is clearly detected (the strong emission line with the longest wavelength in Figures 3 and 4), whose formation height is about 6000 km above the photosphere. This indicates that the pointing of our SP observations ranged from the uppermost layers of the chromosphere to the transition zone. The relative average heights of these four SP spectra can be determined by their corresponding continuum intensity I_c. The 38th frame corresponds to the lowest region, followed by the 35th and 57th frames, with the 99th measuring the polarization produced by the highest domain above the limb.

3. OBSERVATIONAL RESULTS

The most outstanding characteristics shown in Stokes Q/I and U/I maps in Figure 2 are the high degree of polarization, with a maximum of 76.2% for Stokes U/I and 57.4% for Stokes Q/I. Such high polarization degrees have been reported by many IP observers (especially by Koutchmy & Schatten 1971; Badalyan & Sýkora 1997). The variation in polarization with quadrant is also evident. The positive and negative polarizations appear alternatively twice over the four quadrants. This pattern clearly shows evidence that the polarization direction distribution is synoptically parallel to the local solar limb. The variation phase lag between these two Stokes parameters is about 45°, consistent with the definition of Stokes parameters. The difference d between the polarization direction and the local tangential direction (see the lower-right panel of Figure 2) is expressed by

$$\begin{aligned}\sin 2d \equiv\ & \sin(2\chi' - 2\chi) = U/\sqrt{(Q^2+U^2)} \\ & \times \cos 2\chi - Q/\sqrt{(Q^2+U^2)} \times \sin 2\chi \\ \equiv\ & (U\cos 2\chi - Q\sin 2\chi)/LP, \end{aligned} \quad (1)$$

where χ' and χ represent respectively the polarization direction and the angle of the local tangential direction with respect to the reference positive direction of Stokes Q. This map is valuable because it reflects the change of the polarization direction due to local structures. It seems that each loop system can change

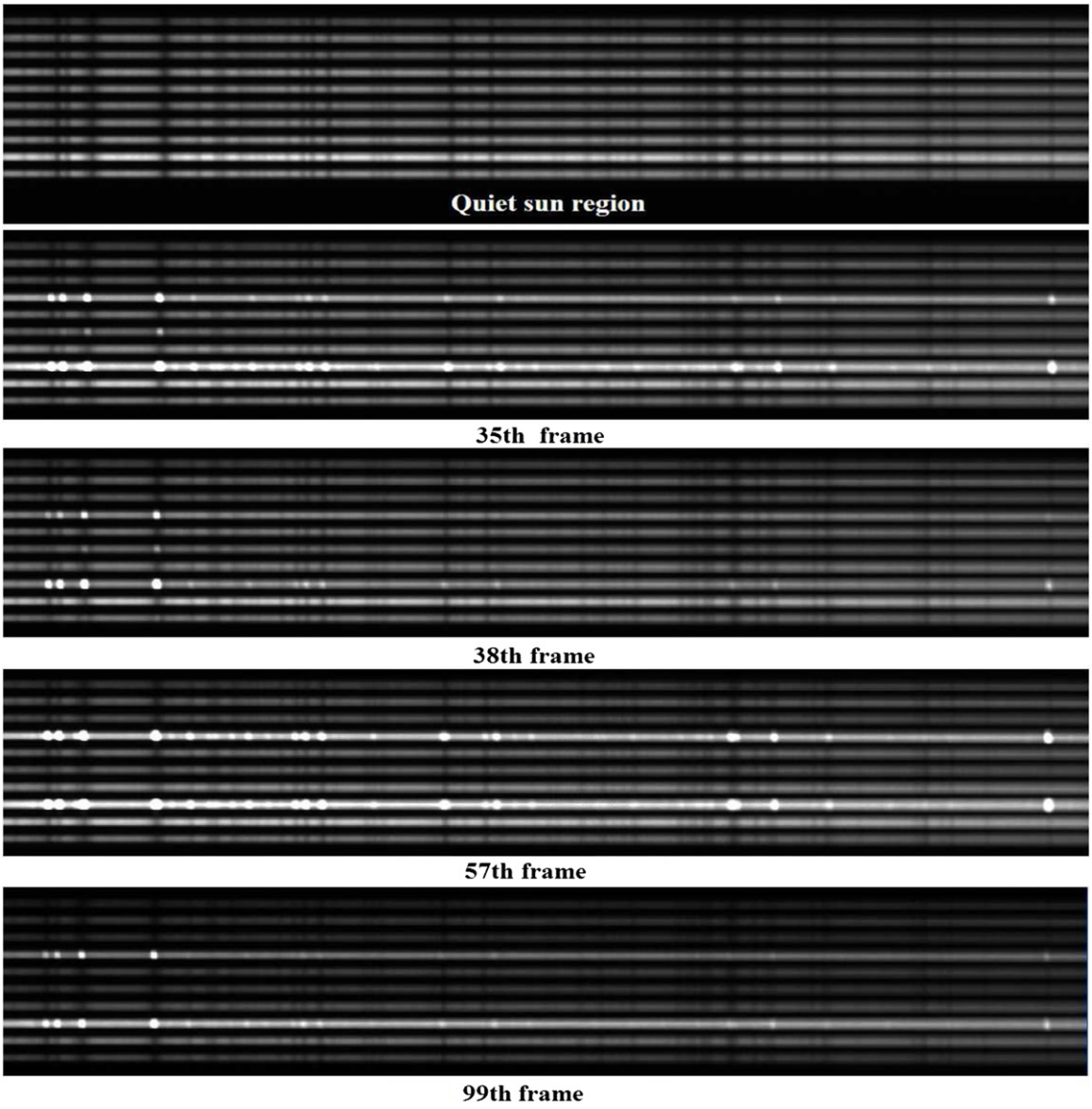

Figure 3. Raw data acquired just before the second contact of the solar eclipse in 2010. The polarimetric pair consisting of the fourth and eighth fiber, counted from the top to bottom in each panel, is used for further reduction. The wavelength increases from left to right and the magnesium triplet are those strong emission lines in the short wavelength region.

the polarization direction almost consistently in the same way. This map provides higher contrast between these structures and the background than that shown by the Stokes I map (lower right panel of Figure 1) and therefore can be used for identifying the fine structures above the limb. It is evident that the departure from the background is also seen from the total linear polarization map (lower left panel in Figure 2), but the departure does not supply the same remarkable difference that $\sin 2d$ provides. For instance, these structures close to the southwest limb can only be clearly recognized when they become obscure in the LP/I map and invisible in the Stokes I map, and so do these loop systems just above the limb which are so prominent and ubiquitous. From this map, we may conclude that the upper solar atmosphere is dominated by abundant loop systems, closed or well-extended, of small scale or large scale. However, because the single beam polarimetry suffers from seeing-induced spurious small-scale signals (Casini et al. 2012), some of the structures like the crossed fibrils at the southeastern limb may not be genuine. It is easily seen in the LP/I map that the background polarization increases with height, and that the solar features above the limb are darker than the background in the map, which means the total linear polarization amplitudes changed by these features are smaller than those of the background. This scenario was also observed by, say, Badalyan & Sýkora (1997).

Another synoptic feature again reported by other observers is that the polarization degree increases with height as a whole. The evidence can be found intuitively from the maps of Stokes Q/I, U/I, and LP/I. More direct evidence is shown in Table 1, which presents the height variations. It is outstanding at first glance that the polarization amplitudes reach high levels. Even in the innermost annulus formed from 0.05 $R_{\rm sun}$ to 0.1 $R_{\rm sun}$, the maximum amplitude that can be achieved is 48.0% for Q/I and 53.8% for U/I; the maximum polarization degree that can be reached 77.5%. Both the average and maximum total linear polarization degrees, independent of the coordinates defining Stokes Q and U, increase with height until 0.4 $R_{\rm sun}$. The averaged values (labeled by "Aver" in the table) are defined

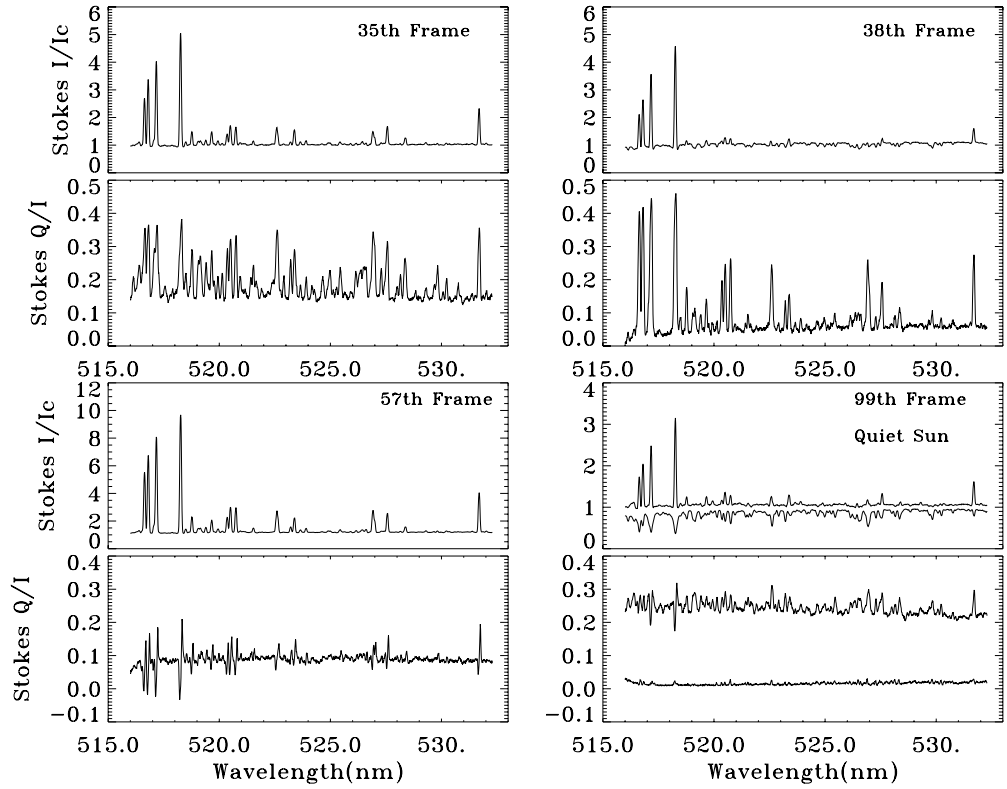

Figure 4. Sample Stokes spectra derived from the polarimetric pair (4, 8) shown in Figure 3 and the polarimetric error bar curve (the lowest curve in the bottom right panel).

Table 1
Height Variation of Polarization Degrees

Height Range[a]	Aver Q/I	Max Q/I	Min Q/I	Aver U/I	Max U/I	Min U/I	Aver LP/I	Max LP/I
0.05–0.10	−0.004	0.480	−0.379	−0.007	0.538	−0.476	0.285	0.544
0.10–0.20	0.016	0.547	−0.505	0.013	0.686	−0.516	0.371	0.719
0.20–0.30	0.098	0.577	−0.474	0.142	0.731	−0.496	0.422	0.740
0.30–0.40	0.166	0.519	−0.285	0.254	0.775	−0.401	0.472	0.778
0.40–0.50	0.141	0.265	−0.016	0.341	0.739	−0.075	0.496	0.756
0.05–0.65	0.035	0.577	−0.505	0.064	0.775	−0.516	0.355	0.778

Note. [a] In units of solar radius $R_\odot$.

as the sum of the polarization degrees over those spatial points possessing non-zero polarization divided by the total number of these points. If the average value equals zero, it implies that positive and negative polarizations cancel out and reflects a kind of symmetry of polarization distribution. It is evident that this symmetry is gradually broken with height for both Stokes Q/I and U/I. It is noteworthy that the maximum amplitudes of Stokes Q/I, U/I, and LP/I within 0.10 solar radius above the limb can reach 48%, 54%, and 55%, respectively, but the average value of LP/I reads as 28.5%. These results are consistent with those derived from the SP below.

In the last row of Table 1, an overall evaluation of these parameters over the observable domain is presented. From these results and the maps of Figure 2, we conclude that an intrinsic property of the upper solar atmosphere is that it is highly polarized, and that the solar structures above the limb change the regularly distributed background polarization greatly both in amplitude and directions. Further the distribution of polarization degrees are highly scattered over the observable domain. Although the evidence in the distribution of linear polarization is easy to see, it is difficult to tell how different chemical elements contribute to the polarization using only IP. To answer these questions one needs SP.

Figure 4 presents Stokes I/I_c and Q/I profiles in different ionization states derived from Figure 3. This shows that many flash lines of many elements such as Fe I, Fe II, Mg I, Nd I, etc., exhibit very high linear polarization >30% up to ≃50%. The contributions to the integrated Q/I over the band vary between frames. Some weak lines also contribute significantly to the overall polarization in frames 35 and 38, but their contributions are negligible in frames 57 and 99. In frame 38, the Q/I integrated over the band comes mainly from the polarization of the lines, while in frame 35, the contributions to the polarization from the lines and from the continuum are close. In contrast to the cases of frames 35 and 38, the flash spectral lines contribute much less to the polarization in frames 57 and 99 than the continuum. The contribution to Q/I from even the strong lines is not significant in frame 99. In frame 57, Q/I profiles of the strong lines show an approximate anti-symmetry in their polarization amplitude, which is less than that of the continuum in the blue wings but greater in the red wings. This behavior is also seen in frame 99, but only for the magnesium lines at 517.3 nm and 518.4 nm.

It is clear that more interesting behavior can only be investigated by a combination of imaging and spectral polarimetry. Integrating over the band 516 nm–532.5 nm indicates a polarization of 7.9% in the case of frame 38, which is obtained in the lowest layers, while the polarization of the continuum is 3.8%. For frame 35, integration over the band results in a polarization of 18.4% for the spectrum and 14.0% for the continuum. For frame 57, the integrated polarization over the band reads as 8.85%, with negligible contribution from the lines. For frame

99 measured in the highest region, the integrated polarization is 24.3%, but the continuum polarization dominates with 23.2%. This suggests that contribution from neutral atoms decreases with height, as does the contribution of spectral lines from ions while the continuum polarization increases as a general trend. It is noteworthy that all these integrated polarization amplitudes are within the ranges listed in Table 1, which resulted from the IP.

4. DISCUSSIONS AND CONCLUSIONS

We have shown how IP provides a synoptic view of the polarization properties of the upper solar atmospheres. Based on the spatial distribution of polarization, these atmospheres can be divided into two components: the background and the solar structures above the limb, as observed by Badalyan & Sýkora (1997). The background polarization exhibits a regular distribution pattern in which the polarization direction is parallel to the solar limb, with various structures modifying the distribution on different scales. The polarimetric maps, especially the $\sin 2d$ map, are useful to see the systematic variation in polarization direction by the loop systems and, on the other hand, to recognize these solar structures above the limb because of the higher contrast produced by the variation. According to this map, loop systems above the limb are ubiquitous and have various scales and morphologies.

However, spectral polarization provides abundant extra information which is essential for identifying the polarization sources and the underlying physical mechanisms. It tells us that the polarization amplitude varies between atomic species and ionization states from one spectral feature to another. The contribution to the integrated polarization over the band from spectral lines can be comparable to that from the continuum in the inner layers involved, and their contribution decreases with height while the continuum polarization increases and becomes generally dominant in the outer atmosphere.

It is almost impossible to find the quadrant variation in polarization with SP, or to provide variation in polarization profiles from one spectral line to another by IP. Therefore, they are complementary. But more important is that both SP and IP provide consistently inherent evidence that the polarization can exceed 20% even below the corona, and that the integrated values increase with height up to 0.4 solar radius above the limb as a whole. We conclude that it is essential and fruitful to combine imaging and spectral polarimetry.

Finally, we note that the theory currently lags behind the observations. Almost all previously cited authors report very high degrees of polarization. In fact, only a few papers concerning polarization sources and mechanisms responsible for these high polarization degrees have been published. Molodensky (1973) gave an explanation of strong polarization by Thompson scattering by considering high-speed free electrons in the process. He concluded that the extremely strong polarization observed by Koutchmy & Schatten (1971, p. 117) at a height of one solar radius can be caused by "electrons moving toward the Sun with energy of the order $E = 100$ keV–0.5 MeV." However, this can only be responsible for the continuum polarization. For spectral line polarization, only a few special lines were considered until now. Sahal-Bréchot (1974a, 1974b) explored the polarization and depolarization for the forbidden lines due to impact between protons and electrons, especially on the coronal green line, and then on the infrared lines of Fe XIII 1074.7 nm (Sahal-Bréchot 1977). House (1977) presented the theoretical height distribution of linear polarization of the same resonant line. He demonstrated that the linear polarization degree can reach even 65%, which is ascribed to the imbalance of populations among the Zeeman sub-levels with depolarization by collisions. House et al. (1982) employed the same mechanism to investigate the coronal green line, and concluded that the linear polarization degree may reach 30% under the assumption that the magnetic field is radial and weak. Raouafi et al. (1999, 2002) pointed out a mechanism that the partial anisotropy of radiation from the transition zone can create linear polarization, and then Raouafi & Solanki (2003) also presented the influence of anisotropic velocity distribution on linear polarization of the resonant scattering coronal line O VI 103.2 nm in both direction and amplitude. However, we have found in this paper that non-forbidden or non-resonant bound–bound transitions in some environments can also produce strong polarization. One mechanism pointed out by Karlicky & Henoux (2002) is that the directional bombardment in the solar atmosphere can produce polarization degree exceeding 20%. Small-scale jets (De Pontieu et al. 2011) ubiquitous in the upper solar atmospheres may play the role in this directional bombardment source. Recently, Milić & Faurobert (2012) considered scattering polarization of molecular lines of C_2 and MgH in a spherical rather than parallel-plane atmosphere. They revealed that for these two molecular lines, the polarization amplitudes are model dependent, e.g., they can vary from 2% to 10% from one model to another, and so do the heights where the polarization degrees reach maximum. It is also concluded by them that after polarization reaches maximum, the amplitudes experience a little decrease and then an increase again while the continuum polarization increases with height consistently. Finally, the Q/I profiles, which appear in bottom left panel of Figure 4, may provide a clue to the mechanism.

Though it is not a task for us to get into more details of the mechanisms responsible for the observational results, we try to provide some clues here. There are many mechanisms influencing the polarization, among which the role of anisotropy should be more emphasized. For instance, Raouafi & Solanki (2003) found that the anisotropy in macrovelocity distribution can significantly change the polarization properties, and so can the anisotropy of radiation (Raouafi et al. 1999, 2002). Because the physical conditions in the upper solar atmosphere deviate far away from thermodynamic equilibrium, it is reasonable to conclude that the anisotropy of microvelocity distribution can also considerably change both the direction and amplitude of the linear polarization for some spectral lines.

We have only just started to harvest the treasures provided by solar eclipse polarimetry. It is clear that both imaging and spectral polarimetry is required. Ideally, this should be done simultaneously on the same telescope as for the forthcoming FASOT project (Qu 2011), which will provide imaging SP using close-packed lenslet-coupled fiber bundles to provide the imaging capability in conjunction with a high-resolution spectrograph.

This work is sponsored by National Science Foundation of China (NSFC) under the grant numbers 11078005 and 10943002, and China's 973 project under the grant number G2011CB811400. Thanks to Emmy Norton for her precious support and to the referee for constructive comments.

REFERENCES

Badalyan, O. G., & Sýkora, J. 1997, A&A, 319, 664
Blackwell, D. E., & Petford, A. D. 1966, MNRAS, 131, 399
Casini, R., de Wijn, A. G., & Judge, P. G. 2012, ApJ, 757, 45

De Pontieu, S., McIntosh, S. W., Carlson, M., et al. 2011, Sci, 331, 55
Eddy, J. A., & Malville, J. 1967, ApJ, 150, 289
House, L. L. 1977, ApJ, 214, 632
House, L. L., Querfeld, C. W., & Rees, D. E. 1982, ApJ, 255, 753
Hyder, C. L., Mauter, H. A., & Shutt, R. L. 1968, ApJ, 154, 1039
Karlicky, M., & Henoux, J. C. 2002, A&A, 383, 713
Kim, I. S., Lisin, D. V., Popov, V. V., & Popova, E. V. 2011, in ASP Conf. Ser. 437, Solar Polarization, ed. J. R. Kuhn et al. (San Francisco, CA: ASP), 181
Koutchmy, S., & Schatten, K. H. 1971, SoPh, 17, 117
Kulijanishvili, V. I., & Kapanadze, N. G. 2005, SoPh, 229, 45
McDougal, D. S. 1971, SoPh, 21, 430
Milić, I., & Faurobert, M. 2012, A&A, 539, A10
Molodensky, M. M. 1973, SoPh, 28, 465
Ney, E. P., Huch, W. F., Kellogg, P. J., et al. 1961, ApJ, 133, 616
Qu, Z. Q. 2011, in ASP Conf. Ser. 437, A Fiber Arrayed Solar Optical Telescope, ed. J. R. Kuhn et al. (San Francisco, CA: ASP), 423
Qu, Z. Q., Zhang, X. Y., Xue, Z. K., et al. 2009, ApJL, 695, L194
Raouafi, N.-E., Lemaire, P., & Sahal-Bréchot, S. 1999, A&A, 345, 999
Raouafi, N.-E., Sahal-Bréchot, S., & Lemaire, P. 2002, A&A, 396, 1019
Raouafi, N.-E., & Solanki, S. K. 2003, A&A, 412, 271
Sahal-Bréchot, S. 1974a, A&A, 32, 147
Sahal-Bréchot, S. 1974b, A&A, 36, 355
Sahal-Bréchot, S. 1977, ApJ, 213, 887
Schuster, A. 1878, Obs, 2, 262
Skomorovsky, V. I., Trifonov, V. D., Mashnich, G. P., et al. 2012, SoPh, 277, 267
van de Hulst, H. C. 1950, BAN, 11, 135